# NATURAL PIGMENT SENSITIZED SOLAR CELLS BASED ON ZnO-TiO$_2$-Fe$_2$O$_3$ NANOCOMPOSITE IN QUASI-SOLID STATE ELECTROLYTE SYSTEM

Chalachew Mebrahtu[1], Abi M. Taddesse[1*], Girma Goro[2], Teketel Yohannes[3]

[1]Haramaya University, College of Natural and Computational Sciences, Department of Chemistry, P.O. Box 138, Haramaya, Ethiopia
[2]Dire Dawa University, College of Natural and Computational Sciences, Department of Physics, Dire Dawa, Ethiopia
[3]Addis Ababa Science and Technology University, College of Natural Sciences, Department of Chemistry, Addis Ababa, Ethiopia

**ABSTRACT**. Nanocomposites of Zn-Ti-Fe oxide using zinc as a host with different ratios of precursor salts were prepared by co-precipitation method to use as semiconductors for dye sensitized solar cell (DSSC). The as-synthesized nanocomposites were characterized using XRD, SEM-EDX, TEM and UV-Vis spectrophotometer. DSSCs based on the new semiconductors and di-tetrabutylammoniumcis-bis(isothiocyanato)bis(2,2'-bipyridyl-4,4'-dicarboxylato)-ruthenium(II) (N719) dye has been constructed and characterized. Stability towards dissolution of deposited films of semiconductors in the acidic dye and conversion efficiency was obtained in the order of: ZnO(100%) <ZnO(70%)-TiO$_2$(30%) <ZnO(70%)-Fe$_2$O$_3$(30%) <ZnO(60%)-TiO$_2$(20%)-Fe$_2$O$_3$(20%). Natural pigments were also extracted using ethanol and water as solvents from flowers of *Guizotia scabra* and *Salvia leucantha* plants. From UV-Vis spectra analysis all ethanol extracts of natural sensitizers absorb in the visible region. DSSCs were constructed using the natural pigments as sensitizers. The following best device parameter was achieved by the ethanol extract of *Salvia leucantha* and ZnO-TiO$_2$-Fe$_2$O$_3$ nanocomposite semiconductor. When the potential is scanned: a $V_{oc}$ of 280 mV, $J_{sc}$ of 0.01761 mAcm$^{-2}$ at light intensity of 100 mWcm$^{-2}$ were obtained; the maximum IPCE % was 1.7 and 25.7 for the N719 dye and *Salvia luecantha*, respectively.

**KEY WORDS**: Nanocomposite, Co-precipitation method, Semiconductor, Dye sensitized solar cell, Natural pigments, Conversion efficiency

## INTRODUCTION

Dye-sensitized solar cells (DSSCs) have garnered considerable attention within the solar cell community. With comparatively low manufacturing cost, ease of fabrication, and fair solar-to-electrical conversion efficiency, these cells are potential candidates to replace conventional Si-based solar cells in specialized applications [1]. As a key component of DSSCs, the nanoporous electrode shows high surface area, which enables both efficient electron injection and light harvesting. Unfortunately, the nanoporous electrode also introduces the charge recombination which mainly occurs at the electrode/electrolyte interface due to the absence of energy barrier layer [2].

Dye-sensitized solar cells have extensively employed titanium dioxide (TiO$_2$) semiconductor for efficiency development. Towards next evolution, however, design of new semiconductor material is the key for developing high performance DSSCs. Zinc oxide (ZnO) has a band gap and energy level of the conduction band edge close to TiO$_2$ and its electron diffusion coefficient is higher than that of TiO$_2$. As photoelectrode, however, ZnO has such drawbacks that it is chemically unstable and is easily dissolved in acidic and basic solutions and the amount of dye loadings is less than that on TiO$_2$ [3]. To overcome such problems, composite electrodes based

—————

*Corresponding author. E-mail: abi92003@yahoo.com

on the combination of two or more metal oxides have been extensively studied to enhance the DSSC's performance. The most common combinations of metal oxides include $TiO_2$-MgO [4], $TiO_2$-$Nb_2O_3$ [5], ZnO-$TiO_2$ and ZnO-$Al_2O_3$ [6], $SnO_2$-$TiO_2$ [7] and $SnO_2$-ZnO [8]. The use of composite metal oxide anodes is of interest due to their potential to improve the photovoltaic properties of the cells by improving electron transport in the electrode and hence reducing charge carrier recombination. This paper focuses on the use of ZnO-$TiO_2$-$Fe_2O_3$ composite electrodes to assess its potential application for dye sensitized solar cells. ZnO, $TiO_2$ and $Fe_2O_3$ are n-type semiconductors with reported band-gap values in the range of 3.2–3.4 eV for ZnO and $TiO_2$ and 2.1 eV for $Fe_2O_3$ [9].

In order to replace the rare and expensive Ru(II) compounds which are used as commercial dye sensitizers many kinds of organic synthetic dyes and natural pigments have been actively studied and tested as low-cost materials. Natural pigments are substances that can easily be obtained from fruits, vegetables, leaves and flowers through solvent extraction and can be employed in DSSCs. To date, selected chlorophyll derivatives, raw anthocyanin and betalain extracts are the most successful natural sensitizers, resulting in the generation of monochromatic photon to current conversion efficiency exceeding 60% for DSSC [10].

Previously Sisay *et al.* (2012) reported a work on DSSCs based on the natural pigment extracted from *Syzygium guineense* as sensitizer and $TiO_2$ as semiconductor [10]. In this work natural pigment sensitized solar cells based on new semiconductor were constructed and characterized. To the best of our knowledge ZnO-$TiO_2$-$Fe_2O_3$ nanocomposite as semiconductor and natural pigment sensitizers from flowers of *Guizotia scabra* and *Salvia leucantha* plants has not been reported for DSSCs.

## EXPERIMENTAL

*Synthesis of nanocomposite*

Synthesis of nanocomposites was performed according to the procedure developed by Singh *et al.* [11] as follows: a total of ten samples comprising single (ZnO), binary (ZnO/$TiO_2$ and ZnO/$Fe_2O_3$) and ternary mixed oxides (ZnO/$TiO_2$/$Fe_2O_3$) were prepared by co-precipitation method. One or more of the following precursors were used during the synthesis as required: Iron (III) nitrate nonahydrate, $Fe(NO_3)_3.9H_2O$, zinc acetate dehydrate, $Zn(CH_3COO)_2.2H_2O$, and titanium tetrachloride, $TiCl_4$. Ammonium hydroxide, $NH_4OH$, was used as a precipitating agent and ethyl alcohol was employed to wash the precipitate. Aqueous solutions of precursor salts in a various molar compositions (Table 1) were mixed and stirred for 30 min along with slow addition of $NH_4OH$ solution till pH was raised to 7 at which precipitation occurs. Stirring was continued for another 30 min, after which the precipitate was aged for 24 h, followed by drying for 1 h at 80 $^o$C and vacuum filtered. The precipitate was then calcined in three stages: stage I: 30 min at 250 $^o$C, stage II: 30 min at 600 $^o$C and stage III: 1 h at 800 $^o$C. Stepwise calcinations were conducted to avoid thermal shock that might be induced to the samples during calcination. The powders obtained were subjected to XRD characterization the results of which served as a base to select the samples with the smallest crystallite sizes among the binary and ternary nanocomposites for the subsequent use in the construction of dye sensitized solar cells.

*Preparation of pigment sensitizers*

For the commercial dye sensitizer 0.3 mM solution of N719 dye (Aldrich) was prepared using dry ethanol [12]. For the natural pigment sensitizers, fresh flowers of *Guizotia scabra* and *Salvia leucantha* were collected and dried at room temperature in a shade to prevent pigment degradation. After drying for about 2 months, the samples were crushed with micro plant grinding machine to produce the powder of the respective plant materials. The pigment extraction from the powder was performed as follows: 2 g of each powder sample was taken and

soaked in 50 mL of ethanol for extracting using ethanol. The same amount of powder was soaked in 50 mL of water for extracting with water in separate bottle. The solution was stored at room temperature for about 6 h to dissolve the powder completely. Then the solution was filtered with glass filter to separate the solid from the pure liquid.

Table 1. Designation of the as-synthesized powders.

| Sample name | Experimental condition |
|---|---|
| C1 | 100% Zn |
| C2 | 80% Zn and 20% Ti |
| C3 | 70% Zn and 30% Ti |
| C4 | 60% Zn and 40% Ti |
| C5 | 80% Zn and 20% Fe |
| C6 | 70% Zn and 30% Fe |
| C7 | 60% Zn and 40% Fe |
| C8 | 80% Zn, 10% Ti and 10% Fe |
| C9 | 70% Zn, 15% Ti and 15% Fe |
| C10 | 60% Zn, 20% Ti and 20% Fe |

*Characterization of as-synthesized powders*

*X-ray diffraction (XRD) study*

X-ray diffraction patterns of as-synthesized semiconductors were obtained using a Bruker D8 Advance XRD, AXS GMBH, Karisruhe, West Germany using X-ray diffractometer equipped with a Cu target Kα radiation (wavelength 1.5406 Å). The measurements were made at room temperature and the accelerating voltage and the applied current were 40 kV, 30 mA, respectively. The instrument was operated under step scan type with step time and degree (2θ) of 1s and 0.020°, respectively, for the range of 4° to 64°. Based on the XRD result (data not shown), samples with smallest crystallite sizes from binary and ternary nanocomposites were selected for further characterization. Accordingly XRD, SEM-EDX and TEM were conducted for the selected samples C1, C3, C6 and C10.

*Absorption maxima determination*

Absorption spectra measurements of the as-synthesized powders and natural pigments were made using UV-Vis spectrophotometer (Sanyo, SP65, Galanakamp, UK), by scanning over 200-800 nm. Typically, 0.1 g of the calcined sample was dispersed in 50 mL deionized water and UV–Vis diffuse absorption spectrum was recorded by scanning over 200-800 nm. For the natural pigments, water or ethanol was used as a solvent for extraction. 2 g of the natural pigment was soaked in 50 mL of solvent for 6 h and then filtered for the UV-Vis diffuse absorption measurements.

*Scanning electron microscopy (SEM)/energy dispersive x-ray spectroscopy (EDX)*

The morphology of the solids and particle distribution were determined by scanning electron microscopy (SEM) using a Hitachi TM1000 with EDX detector to do the elemental analysis.

*Transmission electron microscopy (TEM)*

The TEM used in this work was TECNAI 200 KV machine, located at EMU, University of Cape Town, South Africa. The TEM characterization needs special sample preparation for imaging the synthesized materials as follows. First, small amount of the synthesized powder was

mixed with methanol and then sonicated for 10 min. Then after, a drop of mixture was placed on copper grid using pipette and allowed the methanol to evaporate. After the methanol has been evaporated the sample was mounted on a sample holder and placed in a machine. The TEM images were acquired and the average particle size was then determined by using Image Jimage processing software [13].

*Construction of the dye sensitized solar cells*

Indium-tin-oxide (ITO) conductive glass sheets ($2.5 \times 1.5$ cm) were first cleaned with acetone (Aldrich), 2-propanol (Riedel-de Haen) and ethanol (Abron Chemicals) for 20 min in each step using ultrasonic bath. Paste preparation was performed as follows: 30 mg of a dispersing agent, polyethylene glycol (PEG) was dissolved in 10 mL of distilled water. 1.8 g of $ZnO$-$TiO_2$-$Fe_2O_3$ powder was continuously grounded by using porcelain mortar to break down the aggregated particle. Then 2 mL of the PEG solution was slowly added to the powder and completely mixed by using the mortar. Finally the paste was ready for deposition. The same procedure was used to prepare the pastes of $ZnO$, $ZnO$-$TiO_2$ and $ZnO$-$Fe_2O_3$. The anode was then separately prepared as follows: four edges of ITO were covered with adhesive tape to control the thickness of the film and to provide non-coated areas for electrical contact. The colloid was applied to one of the free edges of the conducting glass and distributed with a glass rod sliding over the tape-covered edges. After air drying, the electrode was fired for 30 min at 400 °C in a furnace (Carbolite Model ELF 11/14B). Coating of the semiconductor surface with natural pigments was carried out by soaking the film for 2 h in the extracted pigments. After completion of the pigment adsorption, the electrode was withdrawn from the solution under a stream of dry air. Sensitizing of the film surface with commercial dye was carried out by soaking for 30 min for the films of $ZnO$ and $ZnO$-$TiO_2$; 2 h for the films $ZnO$-$Fe_2O_3$ and $ZnO$-$TiO_2$-$Fe_2O_3$ in a 0.3 mM solution of N719 dye in dry ethanol. The coating was done immediately after the high temperature sintering. The electrode was withdrawn from the dye solution and dried using a stream of dry air by a hair dryer.

Oxidized poly(3,4-ethylenedioxythiophene) coated onto ITO was used as a cathode oxidized PEDOT improves the charge transfer between the ITO and $I^-/I_3^-$ redox [14]. The poly(3,4-ethylenedioxythiophene) (PEDOT) film for the a cathode was formed by electrochemical polymerization of 3,4-ethylenedioxythiophene (EDOT) (Aldrich), in a three electrode one-compartment electrochemical cell. The electrochemical cell consisted of a precleaned ITO-coated glass working electrode, platinum foil counter electrode and quasi-Ag/AgCl reference electrode. The solution used for the polymerization contained 0.1 M EDOT and 0.1 M $(C_2H_5)_4NBF_4$ (Aldrich) in acetonitrile (Aldrich). The monomer was used as received. The polymerization was carried out potentiostatically at +1.8 V for 20 s to obtain consistent morphology. At this potential, the electrode surface becomes covered with blue-doped PEDOT film. The cell was then rinsed with acetonitrile and dried in air. The polymer gel electrolyte was prepared as follows: 0.9 M of 1-ethyl-3-methyl immidiazolium iodide (EMIm-I) was added into acetonitrile (Aldrich) under stirring to form a homogeneous liquid electrolyte. In order to obtain a better conductivity, 0.5 M of sodium iodide (BDH) was dissolved in the above homogeneous liquid electrolyte, and then 0.12 M iodine and 35 wt% of PVP (Aldrich) were added. Then, the resulting mixture was heated at 70–80 °C under vigorous stirring to dissolve the PVP polymer, followed by cooling down to room temperature to form a gel electrolyte [15]. Finally, the gel electrolyte was deposited in the form of thin film on top of the dye coated film electrode. The DSSC was completed by pressing against PEDOT-coated ITO glass counter electrode. The constructed DSSC was then mounted in a sample holder inside a metal box with an area of 1 cm$^2$ opening to allow light from the source.

*Measurements of photovoltaic performance*

The PV measurements of the DSSC were performed using a computer controlled CHI630A Electrochemical Analyzer shown in Figure 1. A 250-W tungsten–halogen lamp regulated by an Oriel power supply (Model 68830) was used to illuminate the DSSC. The white light intensity was measured in the position of the sample cell with Gigahertz-Optik $X1_1$ Optometer. The intensity of the incident light was 100 mW/cm$^2$. A grating monochromator (Model 77250) placed into the light path was used to select a wavelength between 300 and 800 nm. The measured photocurrent spectra were corrected for the spectral response of the lamp and the monochromator by normalization to the response of a calibrated silicon photodiode (Hamamatsu, Model S1336-8BK) whose sensitivity spectrum was known. No correction was made for the reflection from the surface of the sample.
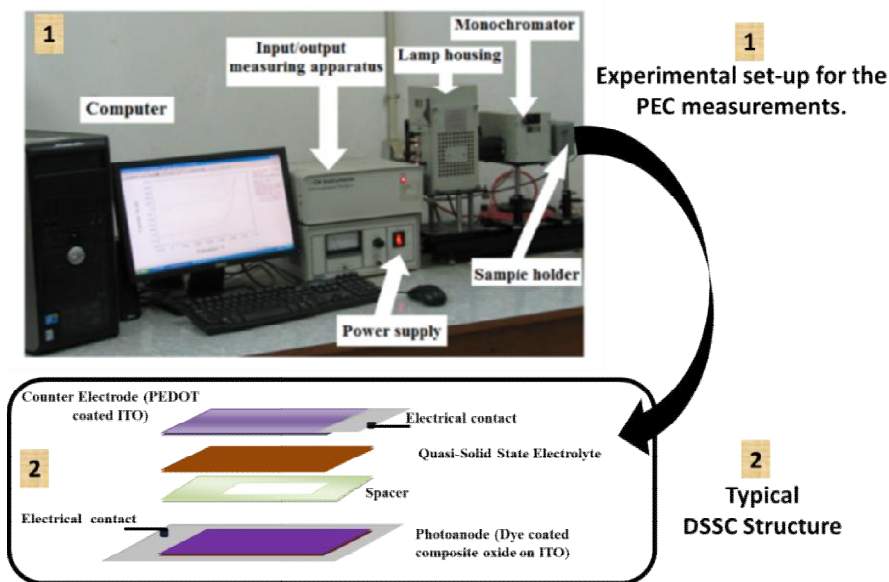


Figure 1. General experimental set-up for the photoelectrochemical (PEC) measurements (1) and typical device structure of the DSSC (2).

Based on the I-V curve, power conversion efficiency (η) was calculated according to equation (1):

$$\eta = \frac{P_{out}}{P_{in}} = \frac{P_{max}}{P_{in}} = \frac{J_m V_m}{P_{in}} = \frac{J_{sc} V_{oc} FF}{P_{in}} \tag{1}$$

where $J_{sc}$ is the short-circuit current density (mA/cm$^2$), $P_{in}$ is the intensity of the incident light (100 mW/cm$^2$), $V_{oc}$ is the open circuit voltage (V), $FF$ is the fill factor defined as:

$$Fill\ Factor = FF = \frac{V_m J_m}{V_{oc} J_{sc}} \tag{2}$$

where $J_m$ and $V_m$ are the optimum photocurrent and voltage that can be extracted from the maximum power point of the current density-voltage (J-V) characteristics [16].

## RESULTS AND DISCUSSION

*XRD analysis*

X-ray powder diffraction of the as synthesized nanomaterials designated as C1 (ZnO), C3 (70%Zn-30%Ti), C6 (70%Zn-30%Fe) and C10 (60%Zn-20%Ti-20%Fe) are shown in Figure 2. The diffraction peaks at scattering angles (2θ): 31.8, 34.5, 36.3, 47.6, 56.6, and 62.9 correspond to the reflection from (100), (002), (101), (102), (110), and (103) crystal planes for ZnO suggesting pure hexagonal wurtzite structure of ZnO. For the Zn-Ti binary nanocomposite (C3), most of the peaks observed in the case of ZnO have also been exhibited evidencing the presence of ZnO in the same phase. In addition to the peaks responsible for ZnO, there are peaks corresponding to 2 theta values of 25.1, 40.2, 54.4 and 62.5 indicating the presence of anatase $TiO_2$. This confirms the formation of Zn-Ti binary nanocomposites the ZnO being the host crystal in agreement with the theoretical composition depicted in Table 1. C6 is another binary phase of Zn-Fe nanocomposite. Additional peaks are observed at scattering angle of 33, 36, 43, 55.6, and 72.5 accounting for hematite phase of $Fe_2O_3$. The diffraction pattern for the ternary Zn-Ti-Fe system (C10) seemed predominantly ZnO although peaks of weak intensity at scattering angles 2 theta of 44.4, 54.5 and 72.5 are shown attributed to anatase/hematite phases. As it has been used elsewhere [17], the average crystalline size of the as-synthesized powders were estimated using Debye-Scherrer equation.
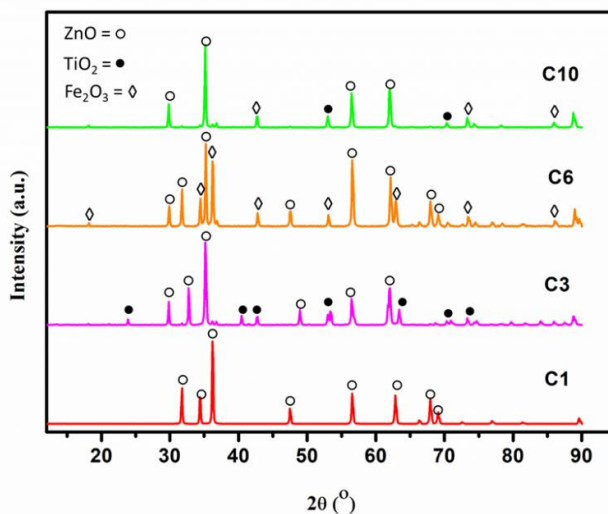


Figure 2. XRD pattern of as-synthesized powders: C1, C3, C6 and C10.

$$D = \frac{K\lambda}{\beta \cos \theta} \tag{3}$$

where D is crystalline size in nm, K is the shape factor constant usually 0.9, β is the full width at half maximum (FWHM) in radians of 2θ, λ is the wavelength of the X-ray which is 0.15406 nm for Cu target $K\alpha_1$ radiation and θ is the Bragg's angle. Using Equation (3), the average crystalline sizes of the as synthesized semiconductors were calculated and given in Table 2. All the as-synthesized powders were found to be in the nano range.

Table 2  Crystal size of as-synthesized powders.

| Nanocomposite | β (radians) | D (nm) |
|---|---|---|
| C1 | 0.00392 | 37 |
| C3 | 0.00699 | 20 |
| C6 | 0.00423 | 34 |
| C10 | 0.00474 | 35 |

D (nm): average crystalline size estimated using Debye Scherer equation.

*UV-Vis absorption spectra analysis*

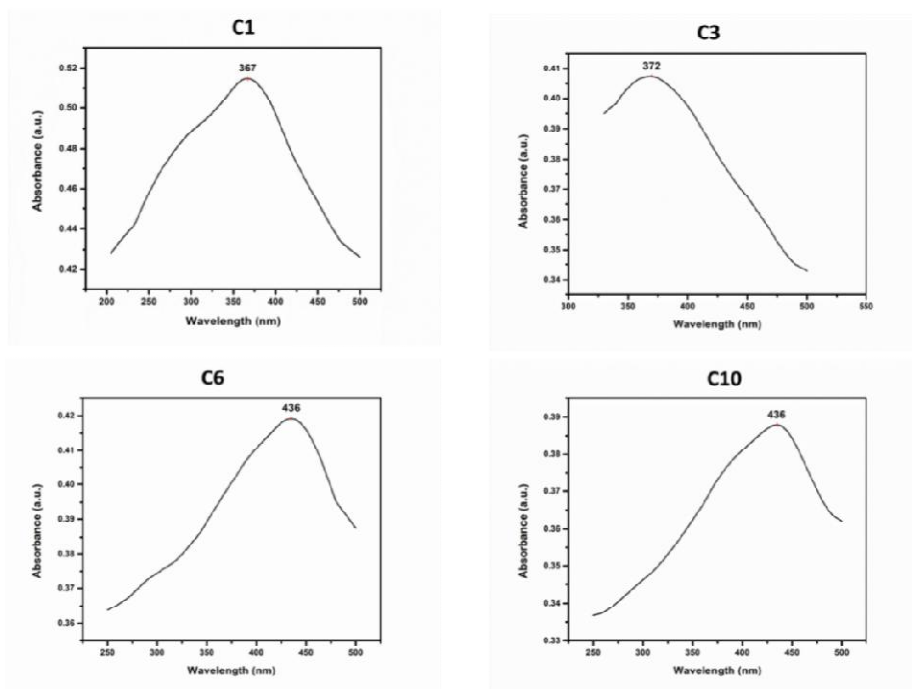UV-Vis absorption spectra for the selected as-synthesized powders are shown in Figure 3.



Figure 1. Uv-Visabsorption spectra of C1 (ZnO), C3 (Zn-Ti), C6 (Zn-Fe) and C10 (Zn- Ti-Fe) semiconductors.

The absorption edges of C6 and C10 nanocomposites showed a remarkable shift to the visible region relative to the pure ZnO (C1). The presence of the narrow band gap hematite could be the reason for the formation of narrow band gap heterojunctions. The binary nanocomposite C3 showed insignificant shift as compared to pure ZnO. In this binary nanocomposite where the components are TiO$_2$ and ZnO, one might expect formation of heterojunctions with little change on the band gap as both semiconductors are wide band gap with relatively closer conduction and valence band edges [18].

Energy bandgap (E$_g$) of the as-synthesized powders were calculated using Equation (4) [19]

$$E_g = \frac{1240\ eV}{\lambda} \tag{4}$$

where, $E_g$ is bandgap energy in electron volts and $\lambda_{max}$ is wavelength (nm) corresponding to maximum absorption.

Critical comparison of the results in Table 3 depicts that the values obtained for the samples having Fe in their composition are remarkably narrowed. The band gap of pure ZnO and $Fe_2O_3$ are 3.2 eV and 2.1 eV [20, 21], respectively. The band gap estimated for ZnO (C1) from Figure 2 is about 3.38 eV confirming the closeness of the value obtained in this work with literature values. No pronounced effect in the band gap has been observed for the binary system Zn-Ti (C3). Unlike C3, the calculated band gap of $ZnO$-$Fe_2O_3$ mixed oxide (C6) was found to be 2.84 eV revealing the red-shift evidenced due to coupling. The energy level of $Fe_2O_3$ both for the valance band and conduction band correspond well within band gap of ZnO contributing for band narrowing due to heterojunction. The same reason could be applied for the ternary system, Zn-Ti-Fe (C10), as well. When the electrons are excited, most of the electron from the conduction band of ZnO can easily transfer to the conduction band of $Fe_2O_3$ this accounts for the reason why the band gap decreased.

Table 3. Wavelength of maximum absorption and energy bandgap of the as-synthesized nanocomposites.

| Samples | Maximum wavelength (nm) | Bandgap ($E_g$) (eV) |
|---|---|---|
| C1 | 367 | 3.38 |
| C3 | 372 | 3.33 |
| C6 | 436 | 2.84 |
| C10 | 436 | 2.84 |

*SEM- EDX spectra analysis*

Scanning electron microscopy was used to observe the morphological features of the selected nanopowders and their corresponding results (SEM images) are presented in Figure 4. According to the SEM images shown in Figure 4, the as-synthesized ZnO (C1) exhibited no distinct morphology except rod-like structures dispersed in the matrix. In the case of binary oxide Zn-Ti (C3), irregularly shaped aggregates of nanoparticles seemed to dominate the structure although remnants of rod-like ZnO with restrained growth are observed. A closer look at the micrograph of C6 (Zn-Fe  binary oxides) also revealed the presence of rod-like structures of ZnO and cubic or pseudo-cubic shaped hematite aggregated in a way that looked like porous in nature in the cluster. The restrained growth of the nanorods could be attributed to the prevailing hematite component in this binary system. The ternary system (Fe-Ti-Fe) (C10) also showed no distinct morphology. The EDX analyses supported the finding evidenced in the XRD. All the metals expected to appear in the binary and ternary systems are observed despite the wider range of elemental compositions indicating the heterogeneity of the nanocomposites (Table S3).

*TEM analysis*

Transmission electron microscopy was used to observe the particle size distribution of the selected nanopowders and accordingly TEM images are presented here under in subsequent Figures (Figure 5 (a to d)) for the four as-synthesized powders.  Particle size analysis from TEM images in Figure 5 using image J image processing software show that all the as-synthesized powders have agglomerates of nano particles. It has also been confirmed that except for ZnO (C1), sizes of Zn-Ti (C3), Zn-Fe (C6) and Zn-Ti-Fe (C10) are 21.59 nm, 30.17 nm and 27.05 nm, respectively. These figures roughly agree with the obtained values from Debye Scherer's

equation that assure the investigated powders are in nano scale which has accounted for their large specific areas.
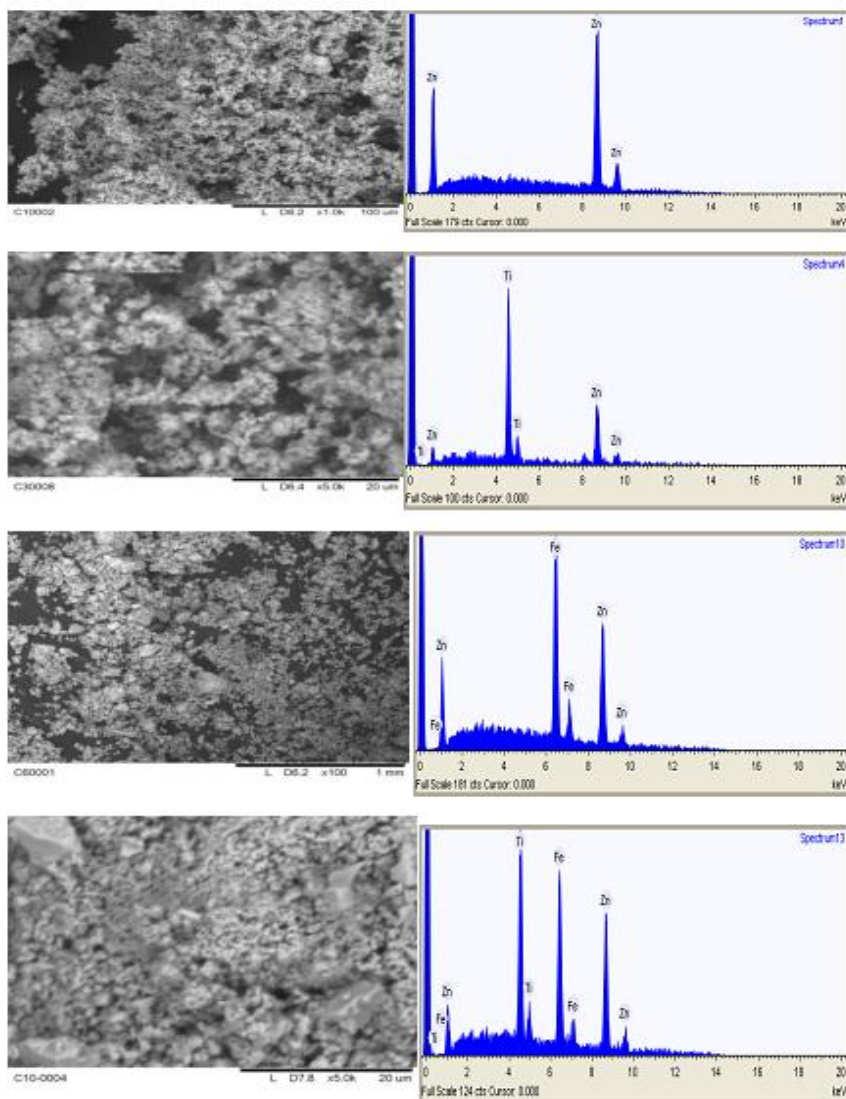


Figure 4. Scanning electron microscopic images of a) C1, b) C3, c) C6 and d) C10.
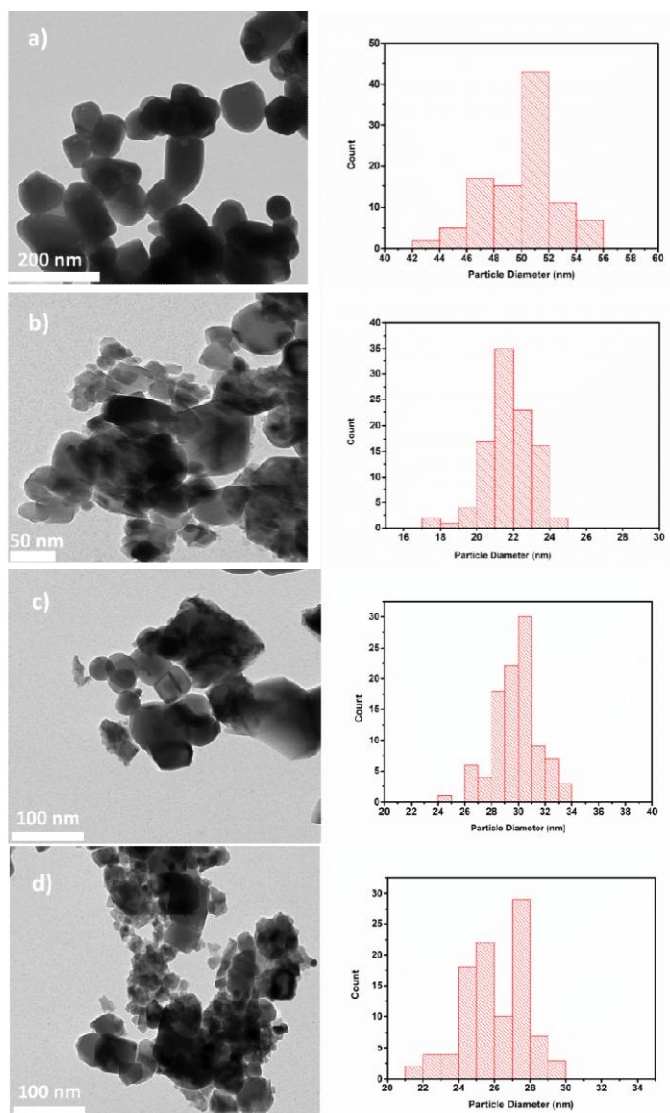
Figure 5. Transmission electron microscopic images and particle distribution of a) C1, b) C3, c) C6 and d) C10.

*Optical absorption measurements of the natural pigments*

The absorption spectra of the extracted natural pigments were measured byUv-Vis spectrophotometer. Accordingly, the absorption spectrum of each sample is shown in Figure 6.

Figure 6. UV-Vis absorption spectra of *Guizotia scabra* extracted with a) ethanol, b) water and *Salvia leucantha* extracted with c) ethanol and d) water.

The ethanol extracts of *Guizotia scabra* and *Salvia leucantha* natural pigments exhibit an absorption peak of about 665 nm and 666 nm, respectively. These absorption peaks indicate the presence of chlorophyll, a group of natural photosynthetic component. As shown in Figure 5, water extract of both flowers does not show any absorption peak, this does not mean that there is no associated pigment. This could be explained based on the shift in equilibrium between the two forms of anthocyanin pigments (flavylium cation, colored and quinonoidal form which is colorless). When the quinonoidal form is dominant, the pigment shows no absorption maxima. This equilibrium can be shifted towards the colored component by simple re-acidification of the extracts. When this sample is acidified an absorption band which is a typical characteristics of anthocyanins starts to be observed due to the shift in equilibrium from quinonoidal to flavylium form. In this type of pigment, the aqueous environment, available in large quantity, adds to the flavyllium form at pH values above 1.5 - 2.0, resulting in a loss of color owing to the formation of the colorless pigment through a slow acid-base equilibrium. This loss of color can be reversed by a simple re-acidification with complete recovery of the colored flavyllium cation (Figure 7). The colorless quinonoidal form of the anthocyanin is largely present in the water extract of all flowers compared to the flavyllium cation form, hence could not show absorption peak for the qualification of the associated pigments. Based on the above reason, absorption spectra measurements of 0.1 M HCl extracts of all the natural dyes were also performed. But it is observed that when both samples are extracted with acid (0.1 M HCl) only *Salvia luecantha* pigment shows an absorption band which is a typical characteristics of anthocyanins due to the shift in equilibrium from quinonoidal to flavylium form.

*Current density-voltage characteristics*

The current density-voltage characteristics of DSSCs constructed based on the four semiconductors sensitized with N719 dye are shown in Figure 8. The device based on ZnO-TiO₂-Fe₂O₃ shows relatively higher current density than the others. This may be attributed to the relatively smaller crystal size and stability of the semiconductor in acidic medium.
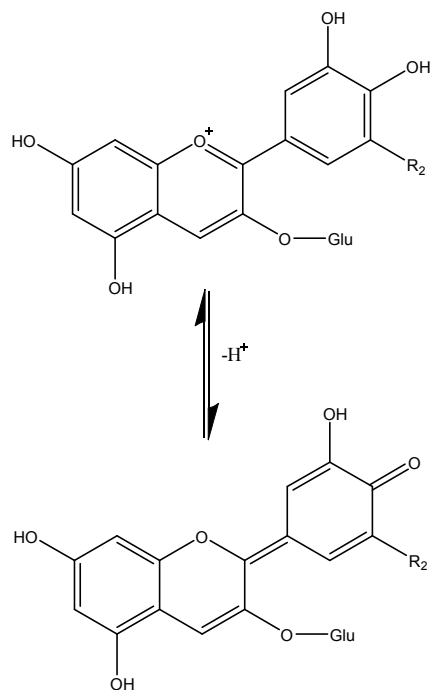
Figure 7. Equilibrium between the flavyllium and the quinonoidal forms in solution.
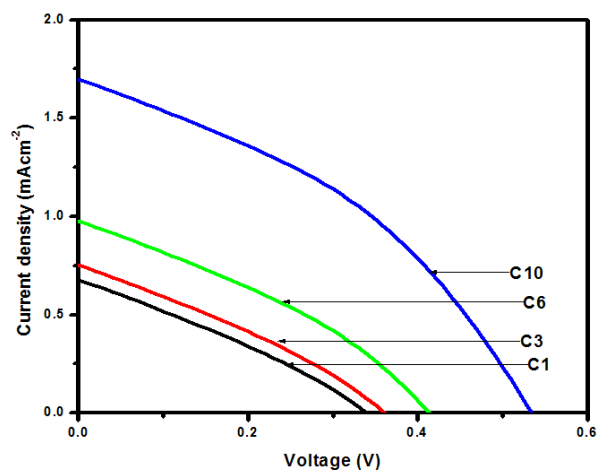


Figure 8. The J-V characteristics of DSSCs based on ZnO (C1), Zn-Ti (C3), Zn-Fe (C6) and Zn-Ti-Fe (C10) sensitized with dry ethanol extracted N719 commercial dye.

The current density-voltage characteristics of DSSCs based on the four semiconductors sensitized with ethanol extracted natural pigments are shown in Figures 9-10. Higher current

density was obtained by the device based on ZnO-TiO$_2$-Fe$_2$O$_3$ semiconductor and *Salvia leucantha* sensitizer.
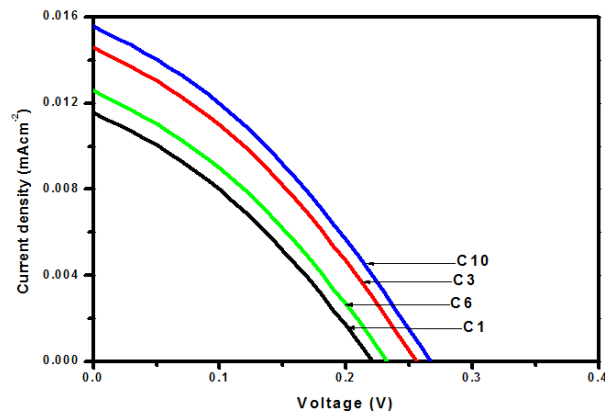


Figure 9. The J-V characteristics of DSSCs based on ZnO (C1), Zn-Ti (C3), Zn-Fe (C6) and Zn-Ti-Fe (C10) sensitized with ethanol extracted *GuizotiaScabra* natural pigment
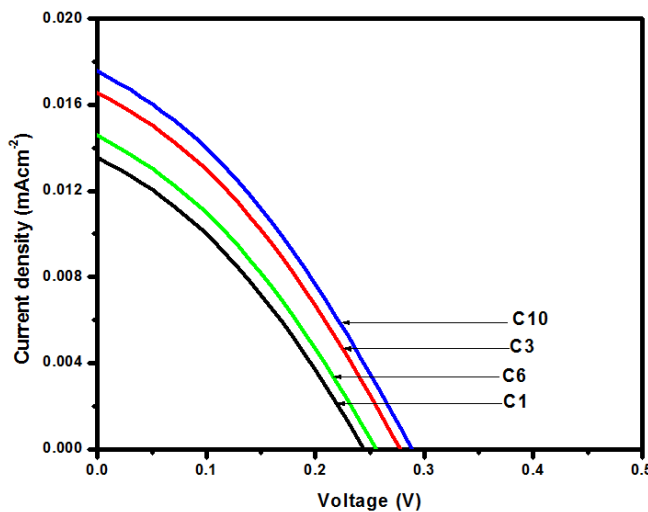


Figure 10. The J-V characteristics of DSSCs based on ZnO (C1), Zn-Ti (C3), Zn-Fe (C6) and Zn-Ti-Fe (C10) sensitized with ethanol extracted *Salvia Leucanta* natural pigment

   The solar energy conversion efficiencies of DSSCs constructed and characterized in this work are given in Table 4. Critical comparison of the conversion efficiency (Table 4) of the as-synthesized semiconductors showed the order: ZnO (C1) < Zn-Ti (C3) < Zn-Fe (C6) < Zn-Ti-Fe (C10). It is known that the commercial dye has acidic nature due to the presence of carboxylic group in its molecular structure which might dissolve the ZnO nanoparticle semiconductor. But it is found that the stability of semiconductor films towards dissolution in acidic dye increases in the following order from the most dissolved one to resistant to the acidic medium: ZnO (C1)

< Zn-Ti (C3) < Zn-Fe (C6) < Zn-Ti-Fe (C10). Formation of heterostructure, therefore, has a role in increasing resistance to acid dissolution apart from the advantage obtained in delaying the recombination of electrons and holes, a distinctive advantage in enhancing the conversion efficiency.

Table 4. Photovoltaic performance of DSSCs based on C1, C3, C6 and C10 sensitized with dry ethanol extracted N719 dye.

| Sensitizer | Semiconductor | $J_{sc}$ (mA.cm$^{-2}$) | $V_{oc}$ (V) | FF % | η |
|------------|---------------|-------------------------|--------------|------|---|
| *N719* | C1 | 0.68 | 0.34 | 29.60 | 0.07 |
| | C3 | 0.75 | 0.36 | 30.70 | 0.08 |
| | C6 | 0.98 | 0.41 | 33.58 | 0.13 |
| | C10 | 1.67 | 0.55 | 37.23 | 0.34 |

Comparison of the solar energy conversion efficiency of the natural sensitizers from Table 5 is obtained in the following order: *Guizotia scabra< Salvia luecanta*. Both natural pigment sensitizers attain the highest efficiency with the ZnO-TiO$_2$-Fe$_2$O$_3$ semiconductor. This is due to the relatively smaller crystallite size and stability of the nanocomposite semiconductor.

Table 5. Photovoltaic performance of DSSCs based on C1, C3, C6 and C10 sensitized with ethanol extracted natural pigments.

| Sensitizer | Semiconductor | $J_{sc}$ (mA.cm$^{-2}$) | $V_{oc}$ (V) | FF % | η |
|------------|---------------|-------------------------|--------------|------|---|
| *Guizotia scabra* | C1 | 0.01157 | 0.22 | 32.84 | 0.00084 |
| | C3 | 0.01457 | 0.24 | 34.21 | 0.0012 |
| | C6 | 0.01257 | 0.23 | 33.32 | 0.00096 |
| | C10 | 0.01557 | 0.25 | 34.82 | 0.0013 |
| *Salvia leucanta* | C1 | 0.01357 | 0.25 | 33.21 | 0.0011 |
| | C3 | 0.01646 | 0.27 | 34.37 | 0.0015 |
| | C6 | 0.01453 | 0.26 | 33.69 | 0.0013 |
| | C10 | 0.01761 | 0.28 | 34.43 | 0.0017 |

*Photocurrent action spectra*

The incident monochromatic photon to current conversion efficiency (IPCE), defined as the number of electrons generated by light in the external circuit divided by the number of incident photons at each wavelength was also studied.

$$IPCE\% = \frac{1240 x J_{SC}[\mu A.cm^{-2}]}{\lambda[nm] x I_{in}[W.m^{-2}]} \tag{5}$$

Photoaction spectra provided further insights on the photoelectrochemical behavior of sensitizers. All the following Figures (Figures 11-13) show the incident photon to current conversion efficiency (IPCE) spectra of ZnO(C1), Zn-Ti (C3), Zn-Fe (C6) and Zn-Ti-Fe (C10) semiconductors sensitized with both N719 dye and extracted natural pigments as a function of wavelength, respectively.

Critical observations of the photocurrent action spectra above the natural pigments show very low sensitization and conversion behavior at the visible region. This may attributed to the low adsorption capacity of ZnO semiconductor which in turn results in low concentration of the natural pigments adsorbed on the surface of the films. But comparing the values, maximum IPCE percentage obtained for the natural pigments was 25.7% at 330 nm by ethanol extract of *Salvia luecanta* based on ZnO-TiO$_2$-Fe$_2$O$_3$ semiconductor. For the commercial dye also the maximum IPCE percentage was found as 1.7% at 330 nm based on ZnO-TiO$_2$-Fe$_2$O$_3$ nanocomposite semiconductor.
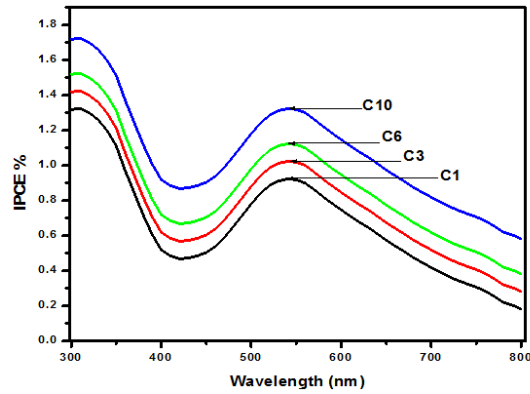
Figure 11. Photocurrent action spectra of based on ZnO (C1), Zn-Ti (C3), Zn-Fe (C6) and Zn-Ti-Fe (C10) sensitized with dry ethanol extracted N719 dye.
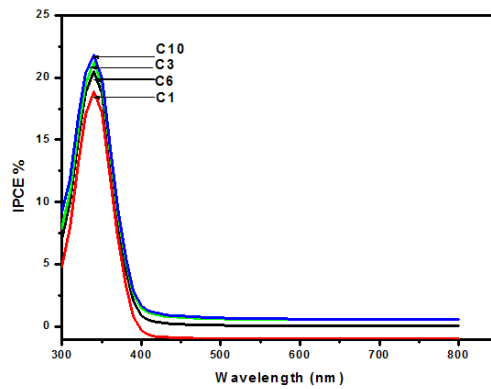


Figure 12. Photocurrent action spectra of based on ZnO (C1), Zn-Ti (C3), Zn-Fe (C6) and Zn-Ti-Fe (C10) sensitized with ethanol extracted *Guizotia scabra* natural pigment.
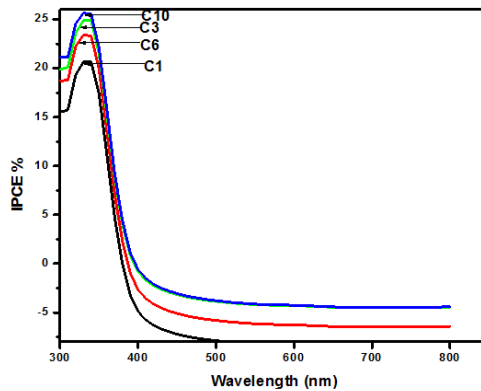


Figure 13. Photocurrent action spectra of based on ZnO (C1), Zn-Ti (C3), Zn-Fe (C6) and Zn-Ti-Fe (C10) sensitized with ethanol extracted *Salvia leucanta* natural pigment.

## CONCLUSION

In this study, a new semiconductor using ZnO-TiO$_2$-Fe$_2$O$_3$ nanocomposite was synthesized, characterized and its property as semiconductor for DSSC was studied using N719 commercial dye as sensitizer. Natural pigments were also extracted from flowers of *Guizotia scabra* and *Salvia leucantha* plants to use as sensitizer pigments for DSSCs constructed based on the new semiconductors. For the N719 sensitizer best performing device with conversion efficiency of 0.34% was obtained using ZnO-TiO$_2$-Fe$_2$O$_3$ nanocomposite as semiconductor. The ternary oxide nanocomposite was also highly resistant to dissolve by the acidic nature of the commercial dye. For the natural pigments the best conversion efficiency and IPCE percentage of *Salvia leucantha* pigment was obtained from the devices constructed based on the ternary oxide (C10) semiconductor. The obtained conversion efficiencies for the ethanol extracts of *Guizotia scabra and Salvia leucantha* were 0.0013% and 0.0017%, respectively. Though the performances of DSSCs under the present experimental conditions are low, the results indicate that it is possible to use ZnO-TiO$_2$-Fe$_2$O$_3$ nanocomposite semiconductor for DSSCs.

## ACKNOWLEDGEMENTS

## REFERENCES

1. Hamann, T.W.; Jensen, R.A.; Martinson, A.B.F.; Ryswyk, H.V.; Hupp, J.T. Advancing beyond current generation dye-sensitized solar cells. *Energy Environ. Sci.* **2008**, 1, 66-78.
2. Wang, Z.S.; Yanagida, M.; Sayama, K.; Sugihara, H. Electronic insulating coating of CaCO$_3$ on TiO$_2$ electrode in dye sensitized solar cell: improvement of electrodes. *Chem. Mater.* **2006**, 18, 2912-2916.
3. Sakai, N.; Kawashima, N.; Murakami, T.N. Effect of TiCl$_4$ treatment on porous ZnO photoelectrodes for dye-sensitized solar cells. *Chem. Lett.* **2011**, 40, 162-164.
4. Bandara, J.; Hadapangoda, C.C.; Jayasekera, W.G. TiO$_2$/MgO composite photocatalyst: The role of MgO in photoinduced charge carrier separation *Appl. Catal. B-Environ.* **2004**, 50, 83-88.
5. Eguchi, K.; Koga, H.; Sekizawa, K.; Sasaki, K. Nb$_2$O$_5$–based composite electrodes for dye-sensitized solar cells. *Bull. Chem. Soc. Jpn.* **2000**, 108, 1067-1071.
6. Law, M.; Greene, L.E.; Radenovic, A.; Kuykendall, T.; Liphardt, J.; Yang, P.D. ZnO-Al$_2$O$_3$ and ZnO-TiO$_2$ core-shell nanowire dye-sensitized solar cells. *J. Phys. Chem. B.* **2006**, 110, 22652-22663.
7. Nasr, C.; Kamat, P.V.; Hotchandani, S. Photoelectrochemistry of composite semiconductor thin films- Photosensitization of the SnO$_2$/TiO$_2$ coupled system with a ruthenium polypyridyl complex. *J. Phys. Chem. B.* **1998**, 102, 10047-10056.
8. Ito, S.; Makari, Y.; Kitamura, T.; Wada, Y.; Yanagida, S. Fabrication and characterization of mesoporous SnO$_2$/ZnO-composite electrodes for efficient dye solar cells. *J. Mater. Chem.* **2004**, 14, 385-390.
9. Xu, Y.; Schoonen, M.A. The absolute energy positions of conduction and valence bands of selected semiconducting minerals. *Am. Mineral.* **2000,** 85, 543-556.
10. Sisay, T.; Atakilt, A; Yonas, C; Garcia, I.V.; Teketel, Y. Natural dye-sensitized solar cells using pigments extracted from *Syzygium guineese J. Photon. Energy* **2012**, 2, 110.

11. Singh, N.; Kumar, P.; Upadhyay, S.; Choudhary, S.; Satsangi, V.R.; Dass, S.; Shrivastav, R. *Synthesis and Characterization of Fe$_2$O$_3$-ZnO Nanocomposites for Efficient Photoelectrochemical Splitting of Water* in *Chemistry of Phytopotentials: Health, Energy and Environmental Perspectives*, Khemani, L.; Srivastava, M.; Srivastava, S. (Eds.), Springer: Berlin; **2012**.

12. Nazeeruddin, M.K.; Kay, A.; Rodicio, I.; Humphry-Baker, R.; Muller, E.; Liska, P.; Vlachopoulos, N.; Graztel, M. Conversion of light to electricity by cis-X2bis(2,2'-bipyridyl-4,4'-dicarboxylate)ruthenium(II) charge-transfer sensitizers (X = Cl⁻, Br⁻, I⁻, CN⁻, and SCN⁻) on nanocrystalline titanium dioxide electrodes. *J. Am. Chem. Soc.* **1993**, 115, 6382-6390

13. Girish, V.; Vijayalakshmi, A. Affordable image analysis using NIH Image/ImageJ. *Indian J. Cancer.* **2004**, 41, Article ID 47.

14. Teketel, Y.; Inganäs, Ö. Photoelectrochemical studies of the junction between poly[3-(4-octylphenyl)thiophene] and a redox polymer electrolyte *Energy Mater. Sol. Cells*. **1998**, 51, 193-202.

15. Fan, L.; Kang, S.; Wu, J.; Hao, S.; Lan, Z.; Lin, J. Quasi-solid state dye-sensitized solar cells based on polyvinylpyrrolidone with ionic liquid. *Energ. Sourc. A*. **2010**, 32, 1559-1568.

16. O'Regan, B.; Grätzel, M. A low-cost, high-efficiency solar cell based on dye-sensitized colloidal TiO$_2$ films. *Nature* **1991**, 353, 737-740.

17. Sasirekha, N.; Rajesk, B.; Chen, W. Synthesis of TiO$_2$ sol in a neutral solution using TiCl$_4$ as precursor and H$_2$O$_2$ as an oxidizing agent. *Thin Solid Films* **2009**, 518, 36-42.

18. Laxmi, J.T.; Chakrabarty, B.S. Synthesis, structural and optical properties of TiO$_2$-ZrO$_2$ nanocomposite by hydrothermal method. *Adv. Mat. Lett.* **2013**, 4, 64-67.

19. El-Kemary, M.; El-Shamy, H.; El-Mehasseb, I. Photocatalytic degradation of ciprofloxacin drug in water using ZnO nanoparticles. *J. Lumin.* **2010**, 130, 2327-2331.

20. Nibret, A.; Yadav, O.P.; Diaz, I.; Taddesse, A.M. Cr-N Codoped ZnO Nanoparticles: Synthesis, Characterization and Photocatalyrtic activity for degradation of Thymol Blue. *Bull. Chem. Soc. Ethiop.* **2015**, 29, 247-258.

21. Maya-Trevino, M.L.; Guzman-Mar, J.L.; Hinojosa-Reyes, L.; Ramos-Delgado, N.A.; Maldonado, M.I.; Hernandez-Ramirez, A. Activity of the ZnO-Fe$_2$O$_3$ catalyst on the degradation of dicamba and 2,4-D herbicides using simulated solar light. *Ceram. Int.* **2014**, 40, 8701-8708.